Paleoceanography and Paleoclimatology

RESEARCH ARTICLE
10.1029/2020PA003991

Special Section:
The Miocene: The Future of the Past

Warm High-Elevation Mid-Latitudes During the Miocene Climatic Optimum: Paleosol Clumped Isotope Temperatures From the Northern Rocky Mountains, USA

K. Methner[1,2], A. Mulch[1,3], J. Fiebig[3], E. Krsnik[1], N. Löffler[1], D. Bajnai[3,4], and C. P. Chamberlain[2]

[1]Senckenberg Biodiversity and Climate Research Centre, Frankfurt am Main, Germany, [2]Department of Geological Sciences, Stanford University, Stanford, CA, USA, [3]Institute of Geosciences, Goethe University, Frankfurt am Main, Germany, [4]Institute of Geology and Mineralogy, University of Cologne, Cologne, Germany

Abstract Interrupting a long-term Cenozoic cooling trend, the Miocene Climatic Optimum (MCO; ca. 17–15 Ma) represents a time interval characterized globally by warmer than present temperatures, lower ice volume, and elevated pCO_2 levels. Establishing quantitative Neogene temperature estimates is an important element in the effort to explore the long-term changes in the carbon cycle and associated climate feedbacks, yet terrestrial temperature records are still sparse. Here, we present a clumped isotope (Δ_{47}) temperature record of the MCO from intermontane basins in the Northern Rocky Mountain (NRM) region. Arikareean (22.7–21.5 Ma) to Barstovian (16.9–14.7 Ma) paleosol carbonates from the Hepburn's Mesa Formation (Montana), supplemented with data from fossil localities in western Idaho. These records yield Δ_{47}-temperatures ranging from 17°C to 24°C, which are rather warm given the high elevation sites and are further relatively stable (mean of 21 ± 2°C) leading into and during the MCO until ca. 14.7 Ma. At ca. 14.7 Ma, we observe low Δ_{47}-temperatures (8°C–10°C) concomitantly with elevated Δ_{47}-temperatures (ca. 22°C). In line with recently suggested climate stability in the NRM region leading into the MCO, our Δ_{47}-temperature record, combined with carbon isotope ($\delta^{13}C$) and reconstructed soil water oxygen isotope ($\delta^{18}O_{sw}$) values, indicates rather stable climate and environmental conditions throughout the MCO. Combining available records from inland sites in the western United States (NRM, Mojave region) points to prevailing stable continental climates even during the MCO.

Key Points:

- First paleosol carbonate clumped isotope (Δ_{47}) temperature record of the Miocene Climatic Optimum in the Northern Rocky Mountain region
- Overall constant Δ_{47}-temperatures (21 ± 2°C) during the Miocene Climatic Optimum until 14.7 Ma
- Constant temperatures suggest dominant continentality and suppressed westerlies

Supporting Information:

Supporting Information may be found in the online version of this article.

Correspondence to:

K. Methner,
kmethner@stanford.edu

Citation:

Methner, K., Mulch, A., Fiebig, J., Krsnik, E., Löffler, N., Bajnai, D., & Chamberlain, C. P. (2021). Warm high-elevation mid-latitudes during the Miocene Climatic Optimum: Paleosol clumped isotope temperatures from the Northern Rocky Mountains, USA. *Paleoceanography and Paleoclimatology*, *36*, e2020PA003991. https://doi.org/10.1029/2020PA003991

Received 28 MAY 2020
Accepted 26 MAY 2021

1. Introduction

The Miocene Climatic Optimum (MCO), a ca. 2 million-year (ca. 17–15 Ma) warming period during the Miocene, reflects the last long-term interruption of Cenozoic cooling (De Vleeschouwer et al., 2017; Zachos et al., 2001, 2008). Elevated pCO_2 levels during the MCO (Breecker & Retallack, 2014; Foster et al., 2012; Kürschner et al., 2008; Sosdian et al., 2018; Steinthorsdottir et al., 2021; Super et al., 2018; Zhang et al., 2013) are in line with elevated temperatures on land (e.g., Böhme, 2003; Ivanov et al., 2011; Larsson et al., 2011; Methner et al., 2020; Pound et al., 2012; Wolfe, 1994) and in the oceans (e.g., Lear et al., 2015; Sosdian et al., 2020; Super et al., 2020, 2018; Zhang et al., 2013). Benthic foraminifera oxygen isotope ($\delta^{18}O$) values document periods of rather rapid temperature change and continental glaciation during the overall warm MCO (MI-2 interval) and into the subsequent Middle Miocene Climate Transition (MMCT; MI-3a and MI-3b intervals) (Diester-Haass et al., 2009; Flower & Kennett, 1995; Holbourn et al., 2013, 2015; Kochhann et al., 2016; Miller et al., 1991; Miller & Mountain, 1996; Tian et al., 2013). In contrast, details of the temperature dynamics in continental environments are still elusive, and it remains unclear how continental temperatures developed into, during, and out of the MCO and how ocean-continent teleconnections may have affected climate in the continental interiors.

In western North America, terrestrial paleoclimate records (paleofloral and conventional stable isotope data) provide evidence for long-term middle Miocene warming (Axelrod & Bailey, 1969; Chase et al., 1998; Mix & Chamberlain, 2014; Pound et al., 2012; White et al., 1997; Wolfe, 1994). Few sections, however, cover significant portions of the MCO (Harris, Strömberg, Sheldon, Smith, & Ibañez-Mejia, 2017; Harris et al., 2020; Loughney et al., 2019; Smiley et al., 2018) and provide quantitative terrestrial temperature estimates (Harris et al., 2020; Huntington et al., 2010; Retallack, 2007). Here, we address this lack of quantitative MCO temperature estimates in western North America by obtaining a high-elevation (e.g., Chamberlain et al., 2012;

Mix et al., 2011) paleosol-based carbonate clumped isotope (Δ_{47}) temperature record from the Hepburn's Mesa Formation (Paradise Valley, MT; ca. 16.5–14.9 Ma). Δ_{47} thermometry on pedogenic carbonates has already provided information on the Late Cretaceous-to-Early Cenozoic terrestrial temperature history, temperature seasonality, as well as hydrological changes of sub-humid to arid settings in western North America (e.g., Burgener et al., 2019; Fan et al., 2017; Hyland et al., 2018; Kelson et al., 2018; Methner et al., 2016; Snell et al., 2013) and, therefore, promises to successfully explore on the Miocene temperature evolution of the Northern Rocky Mountains (NRM) region.

We establish a Δ_{47}-temperature record of pedogenic carbonate of the Late Hemingfordian to Barstovian (ca. 16.5–14.7 Ma) Hepburn's Mesa Formation (Paradise Valley, MT) and supplement this data with age-equivalent and older (Late Arikareean; ca. 22.7–21.5 Ma) records located further west in the NRM (Cottom Lane and Mollie Gulch; Lemhi Valley, ID). Unlike marine records, our composite high-elevation paleosol Δ_{47}-temperature record shows overall invariant temperature estimates of 21 ± 2°C before and during the MCO until about 15.0–14.7 Ma, arguing for warm but more importantly rather stable (long-term) temperature conditions during the MCO. This contrasts with observed temperature swings at a composite Pacific coastal (paleo-floral based) record (White et al., 1997), but is consistent with continental paleoenvironmental and paleoclimate MCO records (Gallagher & Sheldon, 2013; Harris et al., 2020; Loughney et al., 2019).

2. Geological Setting

By the end of the early Miocene, Basin-and-Range-style faulting opened (half-)grabens in SW Montana and adjacent Idaho that provided accommodation space for Sixmile Creek Formation sediments and established an integrated drainage system (Fritz et al., 2007; Fritz & Sears, 1993; Sears et al., 2009; Sears & Ryan, 2003). The sampled middle Miocene sections in Montana (Hepburn's Mesa) and Idaho (Mollie Gulch and Cottom Lane) are today about 200 km apart (Figure 1a) but share a similar tectonic and depositional history. Paradise Valley (MT), which hosts the Hepburn's Mesa Formation, is the northernmost expression of Basin-and-Range deformation (Burbank & Barnosky, 1990). The lithological and sedimentological record of the Hepburn's Mesa Formation (Barnosky & Labar, 1989) largely resemble those of the Deer Lodge and Big Hole River grabens in SW Montana (Sears & Ryan, 2003), arguing for comparable depositional systems across southcentral to southwestern Montana and adjacent Idaho. Thus, the Hepburn's Mesa Formation is not only time-equivalent to sections in SW Montana/Idaho such as Mollie Gulch and Cottom Lane but shares a similar tectonic and depositional history that allows assessing a combined temperature record for the Northern Rocky Mountain (NRM) region.

2.1. Hepburn's Mesa, MT

The Hepburn's Mesa Formation is restricted to the northern part of Paradise Valley (MT), a NE-SW-trending half-graben bounded by the Beartooth (to the East) and Gallatin (to the West) ranges. The Hepburn's Mesa sediment fill consists of white, pink, and green tuffaceous mudstones, silt- and sandstones (Figure 1b) that are overlain by coarse conglomerates and are capped by Late Miocene basalts (Burbank & Barnosky, 1990). The majority of the sections has been interpreted as shallow lake, saline lake, and mudflat deposition (with evaporites: gypsum, calcite) with some eolian contribution in the northern and southernmost exposures (Barnosky & Labar, 1989). However, throughout the sampled type section at Chalk Cliffs (section CC-North; Barnosky & Labar, 1989), we found numerous horizons with calcareous nodules and abundant root casts in the upper part of the section (Figures 1c and 1d) and argue for repeated soil-forming processes on the mudflats and lakeshores.

Age assignments of the rocks are based on biostratigraphy (Barnosky & Labar, 1989; Burbank & Barnosky, 1990), magnetostratigraphy (Burbank & Barnosky, 1990), and $^{40}Ar/^{39}Ar$ dating of ashes (Barnosky et al., 2007). We sampled the basal part of the type section at Chalk Cliffs, an 18 m sandstone cliff (unit 1) at the base and ca. 30–40 m of the accessible section above (unit 2–3, 11–15; units after Barnosky & Labar, 1989; Burbank & Barnosky, 1990), for carbonate nodules (<8 cm), carbonate concretions (<20 cm) and root casts (Figures 1c and 1d). The age of the sampled section was constructed using the paleomagnetic section of Burbank and Barnosky (1990) with the top of unit 1 (18 m massive sandstone cliff) and unit 14 (volcanic ash layer) as marker horizons. The sampled section starts at the uppermost part of Chron C5Cn.2r

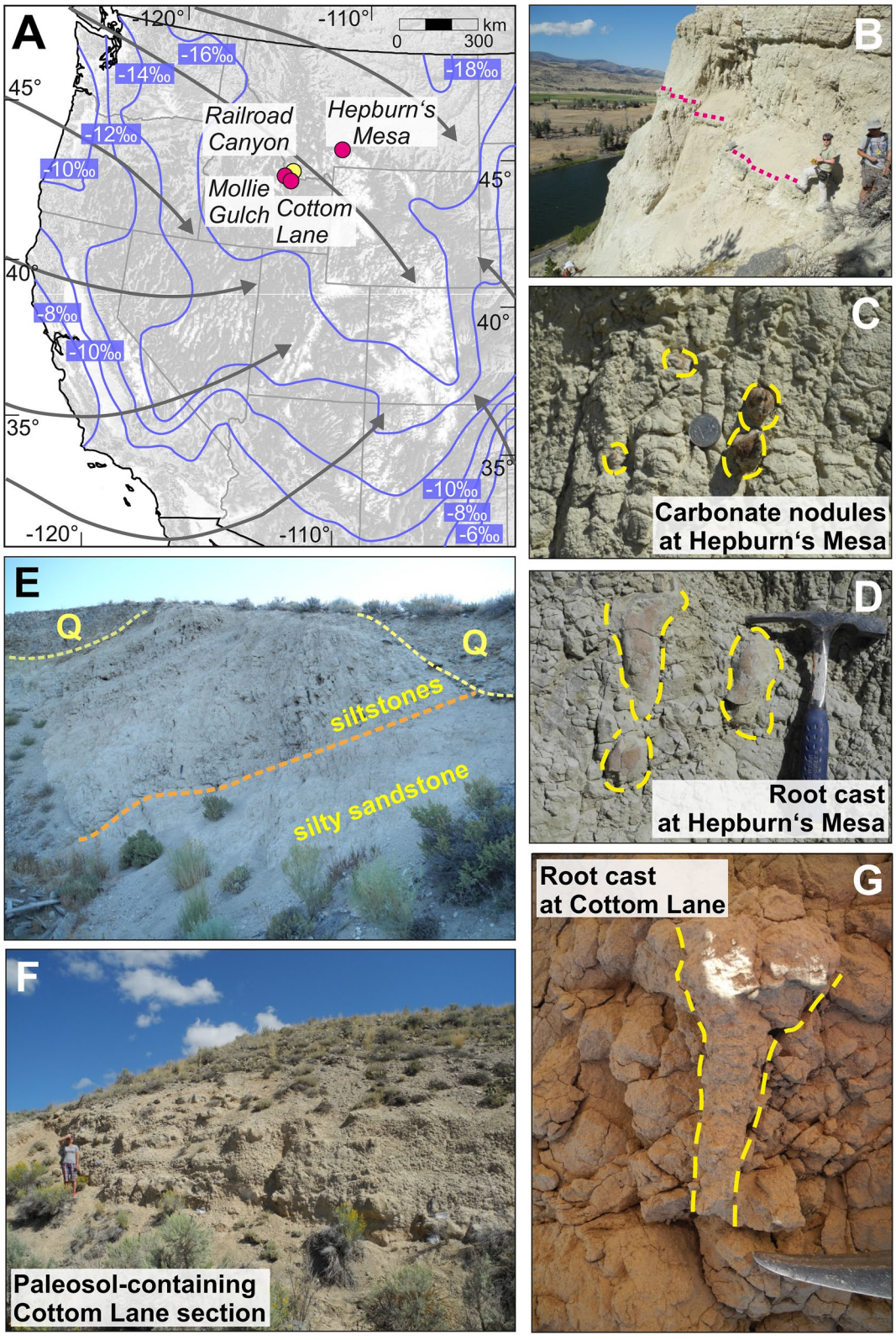
A
-120°
-110°
km
0
300
45°
40°
35°
-16‰
-14‰
-18‰
-12‰
-10‰
-8‰
-6‰
Railroad Canyon
Hepburn's Mesa
Mollie Gulch
Cottom Lane
B
C
Carbonate nodules at Hepburn's Mesa
D
Root cast at Hepburn's Mesa
E
Q
siltstones
silty sandstone
F
Paleosol-containing Cottom Lane section
G
Root cast at Cottom Lane

Figure 1

(16.472 Ma; top of Chron C5Cn.2r) slightly exceeds the top of Chron C5Bn.1n (14.775 Ma; paleomagnetic ages after Hilgen et al., 2012) and thus, spans an age interval of 16.57 Ma to 14.73 Ma. For a detailed assessment of the age constraints, see supplementary information Section S1.1 and Figure S1.

2.2. Lemhi Valley, ID

The Mollie Gulch site sampled here is located in close proximity to the described mammal fossil site (Barnosky et al., 2007; Carrasco et al., 2005) along Old Highway 28 on the Northeastern side of Lemhi Valley (ID). The outcrop consists of a basal unit of pale non-calcareous siltstone overlain by a coarser-grained (~3 m) package of tan silt-/sandstone containing calcareous concretions (2–6 cm) and calcite-cemented (disseminated carbonate) horizons (10–25 cm). The absence of evidence for intensive soil formation (such as carbonate nodules, burrows, root casts, any kind of soil mottling, or slickenside formation) points to carbonate formation from shallow groundwater. The Miocene sediments are unconformably overlain by up to 1 m of Quaternary gravel with modern soil formation from which we obtained modern disseminated carbonates as control samples (Figure 1e).

The lower part of the Mollie Gulch beds is part of the Renova Formation and is overlain by sediments of the Sixmile Creek Formation (Barnosky et al., 2007). The latter yield mammal fossils that have originally been described as latest Arikareean (19.5–18.8 Ma; Tedford et al., 2004) but were later assigned to the Hemingfordian-Early Barstovian (17.5–14.5 Ma; Barnosky et al., 2007). Whitish siltstones or blocky sandy clays are Hemmingfordian (17.5–15.9 Ma) in age and contrast overlying darker sandstones of the early Barstovian (15.9–14.8 Ma) (Carrasco et al., 2005). However, new radiometric data of the nearby Railroad Canyon section (Figure 1a) place the Mollie Gulch locality again well into the Arikareean (Harris, Strömberg, Sheldon, Smith, & Vilhena, 2017). The "early Miocene unconformity" (formerly the mid-Tertiary unconformity), separating the Renova and Sixmile Creek formations, is wide-spread and well recognized across many basins in SW Montana/Idaho (Fields et al., 1985; Hanneman & Wideman, 2006; Harris, Strömberg, Sheldon, Smith, & Vilhena, 2017) and the new age assignments suggest an older age than previously assumed and a very short duration of this unconformity of 21.5–21.4 Ma in the nearby Railroad Canyon section (Harris, Strömberg, Sheldon, Smith, & Vilhena, 2017). Many paleontological age estimates rely on this unconformity and may hence be older than previously thought. Given the location of our sampling site, we consider this section to be part of the older Renova Formation. We, therefore, follow Harris et al. (2020) and place the Mollie Gulch locality at ca. 22.7–21.5 Ma, which is based on the correlation of fossils from Mollie Gulch and those of the dated composite Railroad Canyon section. This makes the sampled Mollie Gulch locality older than the Cottom Lane and Hepburn's Mesa localities and clearly predating the MCO.

The Cottom Lane locality is about 2 km to the NW of Mollie Gulch along Old Highway 28. Here, we sampled a small exposure of tan sediments, mostly clay-to siltstone with abundant paleosol carbonates in the form of nodules, root casts and calcareous horizons (Figures 1f and 1g). Based on recovered fossil taxa this section was assigned a Barstovian-Clarendonian age (15.9–13.0 Ma) (Carrasco et al., 2005). Only one rodent fossil (*Aepycamelus*) has been recovered from this locality, which is regarded to be Early Late Barstovian in age (Barnosky et al., 2007). Correlation to similar fossil remains from the Railroad Canyon section (with revised age) lowers the minimum age to ca. 19.5 Ma (Harris, Strömberg, Sheldon, Smith, & Vilhena, 2017), but the taxon remains present well into the Barstovian (Barnosky et al., 2007; Harris, Strömberg, Sheldon, Smith, & Vilhena, 2017). A more precise age constraint for the samples is currently difficult, but it seems likely that these sediments are younger than the nearby Mollie Gulch section and, given the Hemingfordian to Early Late Barstovian age (Ba1/Ba2 boundary at ~14.8 Ma) of the *Aepycamelus*, are potentially overlapping the younger part of the Hepburn's Mesa section.

Figure 1. Overview map, outcrop situations, and sample examples. (a) Topographic map of the western USA with superimposed modern-day principal storm tracks (gray from Blisniuk & Stern, 2005) and modern river water $\Delta^{18}O$ values (blue contour lines from Kendall & Coplen, 2001). Sampling localities (pink) are the Barstovian Hepburn's Mesa Formation (Paradise Valley, MT, USA), the Barstovian Cottom Lane, and the Arikareean Mollie Gulch fossil localities (both in the Lemhi Valley, ID, USA); composite Railroad Canyon sections shown for reference (yellow); (b) lower ash layer (top marked with stippled line) in the upper part of the Hepburn's Mesa section, serving as a marker horizon for the paleomagnetic section of Burbank and Barnosky (1990) (see supporting information Section 1.1 for age assignments); (c) pedogenic carbonate nodules and (d) root casts from the Hepburn's Mesa Formation; (e) outcrop of Mollie Gulch (Q = Quaternary gravel); (f) outcrop of Cottom Lane, and (g) calcified root cast in the Cottom Lane section.

2.3. Paleoclimate and Paleoenvironmental Setting of the NRM

Middle Miocene temperature records are sparse in the NRM region. Geochemical and paleo-floral based mean annual temperature (MAT) estimates are 10°C–11°C (Railroad Canyon section, 22.9–15.2 Ma; Harris et al., 2020; Retallack, 2007) and 8°C–12°C (NW Idaho locations: Whitebird (Chase et al., 1998), Latah (Wolfe, 1995), Clarkia (Wang et al., 2017)). Overall, arid to semi-arid conditions during the middle Miocene prevail in the NRM region (Barnosky & Labar, 1989; Harris, Strömberg, Sheldon, Smith, & Ibañez-Mejia, 2017; Harris et al., 2020; Retallack, 2007; Strömberg, 2005; Thompson et al., 1982) with precipitation estimates of 300–500 mm/yr (Harris et al., 2020) to 800 mm/yr (Retallack, 2007). Regional and local vegetation reconstructions show open, grass-dominated habitats spreading at the expense of forest cover from the early Miocene onward (Harris, Strömberg, Sheldon, Smith, & Ibañez-Mejia, 2017; Strömberg, 2005, 2011), whereas the paleofloral sites in NW Idaho/E Washington indicate dense vegetation of temperate deciduous forests growing under warm and humid climate (Smiley et al., 1975; Steinthorsdottir et al., 2021; Wolfe, 1995).

3. Methodology

Clumped (Δ_{47}), oxygen ($\delta^{18}O_c$), and carbon ($\delta^{13}C_c$) isotope analyses of pedogenic carbonates were performed at the Goethe University-Senckenberg BiK-F Joint Stable Isotope Facility in Frankfurt (Main), Germany. Each sample was measured with 5–6 replicates and each day 2–3 carbonate reference materials were analyzed alongside sample unknowns. Phosphoric acid digestion of carbonates and purification of extracted CO_2 was performed using HAL (Hofmann's Auto Line) (Fiebig et al., 2019). In brief, pedogenic carbonate powder (8–19 mg) was digested in >106% phosphoric acid at 90 ± 0.1°C for 30 min. The produced CO_2 was purified by passing it through cryogenic traps (−80°C) before and after passage through a Porapak Q-packed gas chromatography column (−15°C) to remove traces of hydrocarbons. The cleaned CO_2 was finally introduced into a ThermoFisher MAT 253 gas-source isotope ratio mass spectrometer (IRMS) and a Thermo Scientific 253 Plus IRMS dedicated to the measurements of masses 44–49. 10–13 acquisitions consisting of 10 cycles each (with an ion integration time of 20 s) were applied to the CO_2 extracted from each replicate.

Alongside sample unknowns and carbonate standards, CO_2 equilibrated at 1,000°C or 25°C were analyzed to monitor the non-linearity of the mass spectrometer and to determine the empirical transfer functions (ETFs) for the projection of raw data to the Carbon Dioxide Equilibrium Scale (CDES) (Dennis et al., 2011). All data was corrected for negative background (Fiebig et al., 2016) and raw Δ_{47}, $\delta^{18}O$ and $\delta^{13}C$ were calculated using the [Brand]/IUPAC parameters (Brand et al., 2010; Daëron et al., 2016). We used the theoretical Δ_{47} of the equilibrated gases, the 25°C–90°C acid fractionation factor, and the Δ_{47}-temperature calibration provided by Petersen et al. (2019) (see supplementary information Section S2 for further details).

Oxygen and carbon isotope ratios were measured using a Finnigan Gas Bench II coupled to a ThermoFisher MAT 253 IRMS. Repeated measurements of an in-house standard (Carrara marble) yielded external precisions of <0.06‰ for $\delta^{18}O_c$ values and <0.02‰ for $\delta^{13}C_c$ values. All isotopic results are reported in standard delta notation and corrected to VSMOW ($\delta^{18}O_c$) and VPDB ($\delta^{13}C_c$). $\delta^{18}O$ values of soil water ($\delta^{18}O_{sw}$) were calculated from paired Δ_{47}-temperatures and $\delta^{18}O_c$ values (see supplementary information Section S2).

4. Results

4.1. Hepburn's Mesa, MT

We sampled Early Barstovian pedogenic carbonates, including carbonate nodules (<8 cm), carbonate concretions (<20 cm) and abundant root casts along the basal part of the type section of the Hepburn's Mesa Formation (section CC-North of Barnosky & Labar, 1989; Figure 1b). We typically analyzed 1–2 samples from the same soil carbonate horizon (Table S2). $\delta^{13}C_c$ and $\delta^{18}O_c$ values of nodules, concretions, and root casts are indistinguishable in their range and mean values. Mean $\delta^{13}C_c$ values are −4.8 ± 0.9‰, −4.9 ± 0.8‰, and −5.4 ± 0.4‰ and mean $\delta^{18}O_c$ values are 15.6 ± 1.3‰, 15.8 ± 1.0‰, and 15.2 ± 1.4‰ for nodules (n = 23), concretions (n = 9), and root casts (n = 7), respectively (Figure 2). We also sampled sparitic calcite (n = 2) along post-depositional fault surfaces that yield a similar mean $\delta^{13}C_c$ value of −5.1 ± 0.1‰, but a significantly lower mean $\delta^{18}O_c$ value of 12.4 ± 1.3‰. For selected samples we sub-sampled profiles of individual nodules, concretions, and root cast in mm-spaced spots (see supplementary information Section S1.2 and

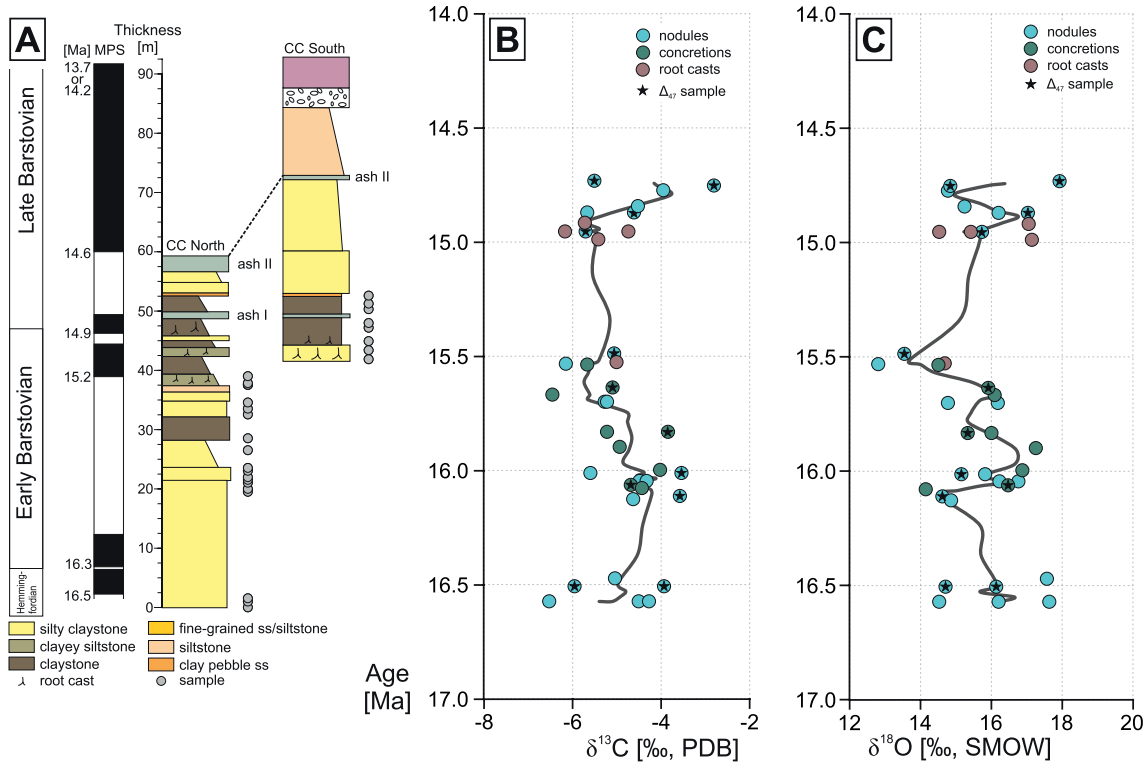

Figure 2. Stratigraphic section and stable isotope data. (a) Stratigraphic and paleomagnetic section of the Hepburn's Mesa Formation type section at the CC-North/South locality (redrawn after Barnosky & Labar, 1989 and Burbank & Barnosky, 1990); gray dots indicate sample positions; (b and c) pedogenic carbonate carbon ($\delta^{13}C_c$) and oxygen ($\delta^{18}O_c$) isotope data of sampled soil nodules (blue), concretions (green), and root casts (brown) with 3pt running average (gray line). Stars highlight samples for clumped isotope analyses.

Figure S2, data set S2). Intra-nodule variability in $\delta^{18}O_c$ and $\delta^{13}C_c$ is relatively low with standard deviations around the mean (SD) of 0.3‰–1.1‰ (for a summary of the data see Table S1). There is no systematic $\delta^{18}O_c$ and $\delta^{13}C_c$ variability across most sub-sampled nodules or concretion (SD < 1.0‰). However, macroscopically different areas such as sparitic inclusions and pale outer rims around the root cast (16-HBM-017) and two nodules (16-HBM-012/16-HBM-020) have $\delta^{18}O$ values that differ by up to 2.5‰ (Data Set S2 and Table S1). Such domains were excluded from further analysis and interpretation. Sampling for clumped isotope measurements was performed only on nodule interiors after cutting open the nodules and gently removing the topmost surface by drilling. This sampling should have avoided any contamination through potentially altered carbonate or carbonate whose formation postdates soil carbonate formation, for example, through dissolution and reprecipitation. Thin section analysis additionally provides evidence that the sampled carbonate domains are micritic (supplementary information Section S1.2 and Figure S2) and thus, most likely pristine.

Δ_{47} values from 9 nodules and 3 concretions range from 0.690 ± 0.006‰ to 0.744 ± 0.010‰ (±1 standard error of the mean), which translate into temperatures of 24.4 ± 2.0°C to 7.7 ± 2.8°C, respectively (Figure 3a; Table 1). Despite one high Δ_{47} value of 0.744 ± 0.010‰ (sample 16-HBM-022A), all other samples fall in a narrow range of 0.690 ± 0.006‰ to 0.712 ± 0.011‰, and hence yield temperatures of 24.4 ± 2.0°C to 17.3 ± 3.7°C, respectively. The one very low temperature of 7.7 ± 2.8°C (sample 16-HBM-022A) differs significantly from an additional nodule from the same horizon, which gave a Δ_{47} value of 0.698 ± 0.009‰ (22.0 ± 3.0°C, sample 16-HBM-022B) and thus falls within the range of the other Δ_{47}-temperature estimates. Similar to the $\delta^{13}C_c$ and $\delta^{18}O_c$ data we do not detect any differences between Δ_{47} values of nodules and concretions that we solely classified based on their size (8–20 cm). In fact, 16-HBM-014 (nodule at 39.0 m of section) and 16-HBM-010 (concretion at 34.5 m of section) sampled in immediate vicinity to each other yield identical Δ_{47} values of 0.700 ± 0.009‰ (21.2 ± 2.9°C) and 0.700 ± 0.008‰ (21.3 ± 2.7°C). The same holds

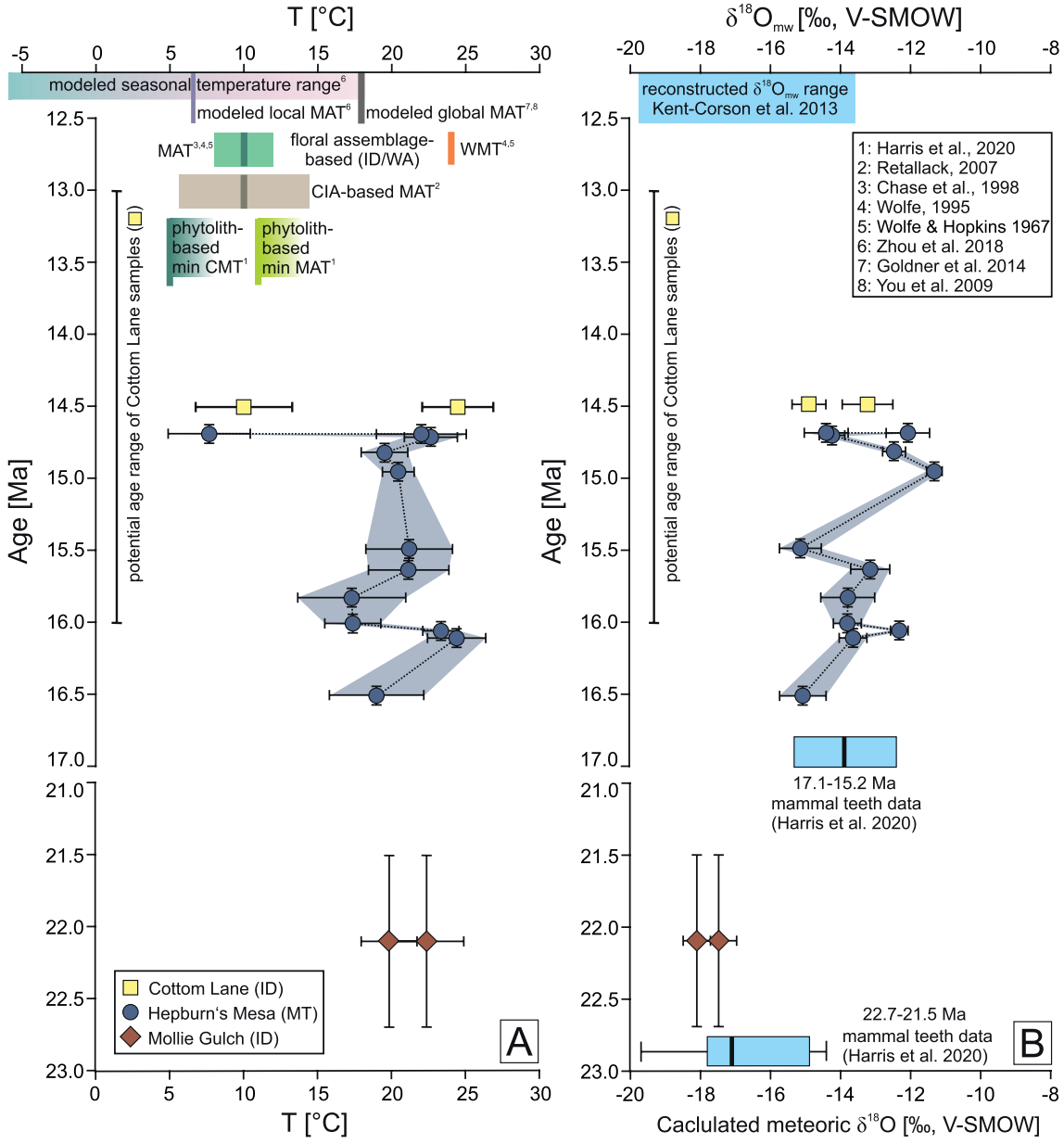

Figure 3. Clumped isotope (Δ_{47}) temperatures and calculated soil water oxygen isotopic compositions ($\delta^{18}O_{sw}$) of Hepburn's Mesa (MT), Cottom Lane (ID), and Mollie Gulch (ID). Δ_{47}-temperatures are calculated using the calibration of Petersen et al. (2019) and $\delta^{18}O_{sw}$ values calculated after Kim and O'Neil (1997) (see Methodology and supplementary information Section S2). (a) Δ_{47}-temperatures compared to temperature records from the Northern Rocky Mountain region based on phytolith analyses (MAT in light green, CMT in dark green; Harris et al., 2020), the chemical index of alteration (Retallack, 2007), paleofloral assemblages (Chase et al., 1998; Wolfe, 1995; Wolfe & Hopkins, 1967), and modeled global mean (Goldner et al., 2014; You et al., 2009) and local temperatures (Zhou et al., 2018). (b) Calculated $\delta^{18}O_{sw}$ compared to meteoric water $\delta^{18}O_{mw}$ estimates based on fossil tooth enamel (Harris et al., 2020) and carbonates (Kent-Corson et al., 2013). $\delta^{18}O_{mw}$ estimates based on teeth enamel are shown for two time-bins after Harris et al. (2020). The Arikareean data are derived from fossils recovered from Mollie Gulch locality, Barstovian data are from the composite Railroad Canyon section (Harris et al., 2020).

for nodule 16-HBM-000 at 23.5 m of section with 0.690 ± 0.006‰ (24.4 ± 2.0°C) and concretion 16-HBM-002 at 24.5 m of section with 0.694 ± 0.004‰ (23.4 ± 1.2°C).

Overall, Δ_{47}-temperatures, excluding 16-HBM-022A, average 20.8 ± 2.2°C (±SD of the mean) (1–56 m). They yield a maximum of 23.9 ± 0.5°C (±SD of the mean) at ca. 16.1 Ma, decrease to 17.3°C–21.3°C (average 19.6 ± 1.7°C) between 26 and 49 m (16.0 Ma and 14.9 Ma) and then slightly increase to temperatures of 22.0°C–22.7°C (22.4 ± 0.3°C, 54–56 m, at ca. 14.7 Ma; excluding sample HBM-022A). However, within error

Table 1
Carbonate Stable ($\delta^{18}O_c$, $\delta^{13}C_c$) and Clumped Isotope (Δ_{47}) Data and Calculated Oxygen Isotopic Ratios of Soil Water ($\delta^{18}O_{sw}$) of Middle Miocene Fossil Sites: Hepburn's Mesa, Cottom Lane, and Mollie Gulch

Sample	Sample type	Strat. height (m)	Age (Ma)	Age error (Ma)	*n*	Mean Δ_{47} (‰)	SE Δ_{47} (‰)	*T* (Δ_{47}) (°C)	SE *T* (°C)	$\delta^{13}C_c$ (‰, VPDB)	$\delta^{18}O_c$ (‰, VPDB)	$\delta^{18}O_c$ (‰, VSMOW)	$\delta^{18}O_{sw}$ (‰, VSMOW)	SE $\delta^{18}O_{sw}$ (‰)
Cottom Lane			13.9–15.9											
16CoL-003B	Nodule	0.5	~14.9	1.0	5	0.736	0.011	10.0	3.3	−6.1	−12.2	18.3	−13.2	0.7
16CoL-004	Nodule	0.6	~14.9	1.0	5	0.690	0.007	24.4	2.4	−5.0	−17.0	13.4	−14.9	0.5
Hepburn's Mesa														
16-HBM-022 A	Nodule	56.1	14.69	0.06	5	0.744	0.010	7.7	2.8	−5.9	−12.9	17.6	−14.4	0.6
16-HBM-022 B	Nodule	56.1	14.69	0.06	5	0.698	0.009	22.0	3.0	−5.6	−13.7	16.8	−12.1	0.6
16-HBM-021	Nodule	54.6	14.71	0.06	5	0.696	0.005	22.7	1.8	−3.0	−16.0	14.5	−14.2	0.4
16-HBM-018 A	Nodule	49	14.82	0.06	5	0.705	0.005	19.6	1.6	−5.3	−13.5	17.0	−12.5	0.3
16-HBM-016 A	Nodule	42.5	14.95	0.06	6	0.702	0.003	20.7	0.9	−5.7	−12.6	18.0	−11.3	0.2
16-HBM-014	Nodule	42	15.49	0.06	6	0.700	0.009	21.2	2.9	−5.2	−16.6	13.9	−15.1	0.6
16-HBM-010	Concretion	34.5	15.64	0.06	5	0.700	0.008	21.3	2.7	−5.1	−14.5	15.9	−13.1	0.6
16-HBM-007 A	Concretion	31.5	15.83	0.06	6	0.712	0.011	17.3	3.7	−4.9	−14.4	16.1	−13.8	0.8
16-HBM-004 B	Nodule	26	16.01	0.06	5	0.712	0.006	17.4	1.9	−4.1	−14.4	16.0	−13.8	0.4
16-HBM-002	Concretion	24.5	16.06	0.06	5	0.694	0.004	23.4	1.2	−5.0	−14.2	16.3	−12.3	0.3
16-HBM-000 B	Nodule	23.5	16.11	0.06	5	0.690	0.006	24.4	2.0	−4.9	−15.7	14.7	−13.7	0.4
16-HBM-025 A	Nodule	1	16.51	0.06	6	0.707	0.010	19.0	3.2	−4.6	−16.0	14.4	−15.1	0.7
Mollie Gulch			21.5–22.7											
16MoG-001	gw concretion	1	~ 22.1	0.6	5	0.697	0.007	22.3	2.5	−6.1	−19.1	11.2	−17.5	0.5
16MoG-005	gw concretion	5	~ 22.1	0.6	5	0.704	0.006	19.8	1.9	−5.7	−19.2	11.1	−18.1	0.4

Note. Δ_{47}-Temperatures are calculated using the AFF and the calibration of Petersen et al. (2019). Δ_{47} errors as the standard error of the mean (SE); *n* gives the number of replicates. $\delta^{18}O_{sw}$ values are calculated by using pairs of Δ_{47} temperatures and $\delta^{18}O_c$ values and oxygen isotope fractionation coefficient of Kim and O'Neil (1997), updated by Kim et al. (2007). Δ_{47}-Temperatures calculated after Wacker et al. (2014) and $\delta^{18}O_{sw}$ values calculated after Coplen (2007) are given in the appendix (supplementary information Table S9).
Abbreviation: gw, groundwater.

the Δ_{47}-temperatures are indistinguishable between 26 to 56 m with a mean of 20.3 ± 1.9°C. Reconstructed soil water $\delta^{18}O_{sw}$ values range from −15.1 ± 0.7‰ to −11.3 ± 0.2‰ (Figure 3b; Table 1). There is no apparent temporal trend in the $\delta^{18}O_{sw}$ record; mean $\delta^{18}O_{sw}$ values of the "warm" interval at 16.1 Ma and the overlying section (16.0–14.7 Ma) are −13.0 ± 0.7‰ and −13.2 ± 1.2‰, respectively, and the entire record yields a mean $\delta^{18}O_{sw}$ value of −13.5 ± 1.2‰.

4.2. Lemhi Valley, ID

At Mollie Gulch, we analyzed three carbonate concretions from sandy siltstone, disseminated carbonate from two calcareous siltstone horizons and two modern soil carbonate samples (disseminated carbonate in the Quaternary cover of the outcrop). The concretions show an average $\delta^{13}C_c$ value of −5.4 ± 0.4‰ and $\delta^{18}O_c$ value of 10.9 ± 0.4‰, which differ slightly from calcareous siltstone horizons with an average $\delta^{13}C_c$ value of −3.4 ± 1.5‰ and $\delta^{18}O_c$ value of 11.9 ± 0.2‰. Modern soil carbonates have a mean $\delta^{13}C_c$ value of −1.1 ± 0.7‰ and $\delta^{18}O_c$ value of 20.4 ± 0.8‰, respectively, and are hence clearly distinct from the underlying Miocene samples (Data Set S2).

The small exposure at the Cottom Lane locality provided abundant pedogenic carbonates and we analyzed seven paleosol nodules, five root casts and disseminated carbonate from two horizons (Data Set S2). Soil nodules and root casts show identical mean $\delta^{13}C_c$ values of −5.9 ± 0.4‰ and −5.9 ± 0.8‰, respectively, whereas the calcareous horizons have distinctively lower mean $\delta^{13}C_c$ values of −7.2 ± 0.04‰. Mean $\delta^{18}O_c$

values are 15.1 ± 2.1‰ (soil nodules), 14.4 ± 0.9‰ (root casts), and 13.7 ± 0.2‰ (calcareous horizons). The $\delta^{18}O_c$ values of the soil carbonates vary from13.3‰ to 18.9‰, whereby only two samples from the same horizon show elevated $\delta^{18}O_c$ values of 17.6‰ and 18.9‰ and the median $\delta^{18}O_c$ values of soil nodules and root casts are identical with 14.2‰ and 14.3‰, respectively.

Due to the difficult age assessment and nature of the carbonate phases of the Mollie Gulch locality (shallow groundwater or incipient pedogenic carbonate), we only analyzed two carbonate samples for Δ_{47} at each of the Lemhi Valley localities. The Δ_{47} values from Mollie Gulch of 0.697 ± 0.007‰ and 0.704 ± 0.006‰ translate into temperatures of 22.3 ± 2.5°C and 19.8 ± 1.9°C, respectively, yielding a mean temperature of 21.1 ± 1.3°C (Figure 3a). The reconstructed $\delta^{18}O_{sw}$ values are identical within error (−17.5 ± 0.5‰ and −18.1 ± 0.4‰) and yield a mean $\delta^{18}O_{sw}$ value of −17.8 ± 0.3‰ (propagated error is 0.6‰) (Figure 3b). This $\delta^{18}O_{sw}$ estimate is consistent with a reconstructed meteoric water $\delta^{18}O$ value based on tooth enamel samples from the same locality (1st time bin after Harris et al., 2020) (Figure 3b). In contrast to Mollie Gulch, the Δ_{47} values at Cottom Lane vary largely with values of 0.690 ± 0.007‰ and 0.736 ± 0.011‰ and associated temperatures of 24.4 ± 2.4°C and 10.0 ± 3.3°C (Figure 3a). Reconstructed $\delta^{18}O_{sw}$ values are −13.2 ± 0.7‰ and −14.9 ± 0.5‰. Interestingly, the reconstructed $\delta^{18}O_{sw}$ values are identical within error with a mean of −14.1 ± 0.8‰ (propagated error is 0.9‰) (Figure 3b). This value, in turn, is similar to the Late Hemingfordian-Early Barstovian median meteoric water $\delta^{18}O$ value, reconstructed from fossil tooth enamel $\delta^{18}O$ values of equids and rhinos from the nearby Railroad Canyon section (time bin 5 after Harris et al., 2020) (Figure 3b).

4.3. A Composite Mid-Miocene Clumped Isotope Temperature Record of the Northern Rocky Mountains

We provide a Δ_{47}-temperature record spanning the MCO based on data from the Hepburn's Mesa Formation (MT) and supplement these with records located further west in the Lemhi Valley (ID) to address terrestrial temperature changes in the NRM region during the middle Miocene (Figure 3a). The two Δ_{47}-temperatures of Mollie Gulch (21.5–22.7 Ma; Harris et al., 2020) show consistent temperatures with a mean of 21± 1°C. Despite the different lithology of the samples, presumably shallow-ground water carbonates, the temperature estimates are identical with those of Hepburn's Mesa (21 ± 2°C) and indicate no major temperature increase entering the MCO (Figure 3a).

The sedimentary section at Hepburn's Mesa covers an age range of 16.5–14.7 Ma and thus much of the MCO including the Mi-2 event (Miller & Mountain, 1996), but not the subsequent MMCT (Figure 4). Overall, Δ_{47}-temperatures are rather constant ranging between 17°C and 24°C until ca. 14.7 Ma (average 21 ± 2°C), excluding the low-temperature sample (8°C) at the top of the section). There are two intervals of increased temperature at ca. 16.1 Ma (23.5–24.5 m) and ca. 14.7 Ma (54.5–56 m) during which temperatures increase to 24°C and 22°C, respectively. Compared to the average temperature of 20 ± 2°C in the intermediate 16.0–14.9 Ma interval (26–49 m) and the basal temperature estimate of 19 ± 3°C at 16.5 Ma, this permits ca. 2°C–5°C warming during select intervals of the MCO.

The pedogenic carbonate samples from Cottom Lane show internally discrepant Δ_{47}-temperatures of 24.4 ± 2.4°C and 10.0 ± 3.3°C but provide consistent $\delta^{18}O_{sw}$ values. Similarly, such a large temperature variability recorded in pedogenic carbonates within a single soil horizon is observed in samples younger than ca. 14.7 Ma at Hepburn's Mesa. These “intra-horizon” Δ_{47}-temperature differences are equally large at Cottom Lane (14.5°C) and Hepburn's Mesa (14.4°C).

5. Interpretation and Discussion

5.1. Middle Miocene Temperature Records of the NRM and Carbonate Formation Seasonality

Combined, paleosol Δ_{47}-temperatures from Montana and Idaho provide a composite NRM Δ_{47}-temperature record that (a) indicates relatively stable soil temperatures of 21 ± 2°C leading into and during the MCO (until about 14.7 Ma) and (b) is consistent with intermittent MCO warming of 2°C–5°C. This record is consistent with proposed stable temperature and environmental conditions between the early and middle Miocene at Railroad Canyon (Harris et al., 2020; Retallack, 2007).

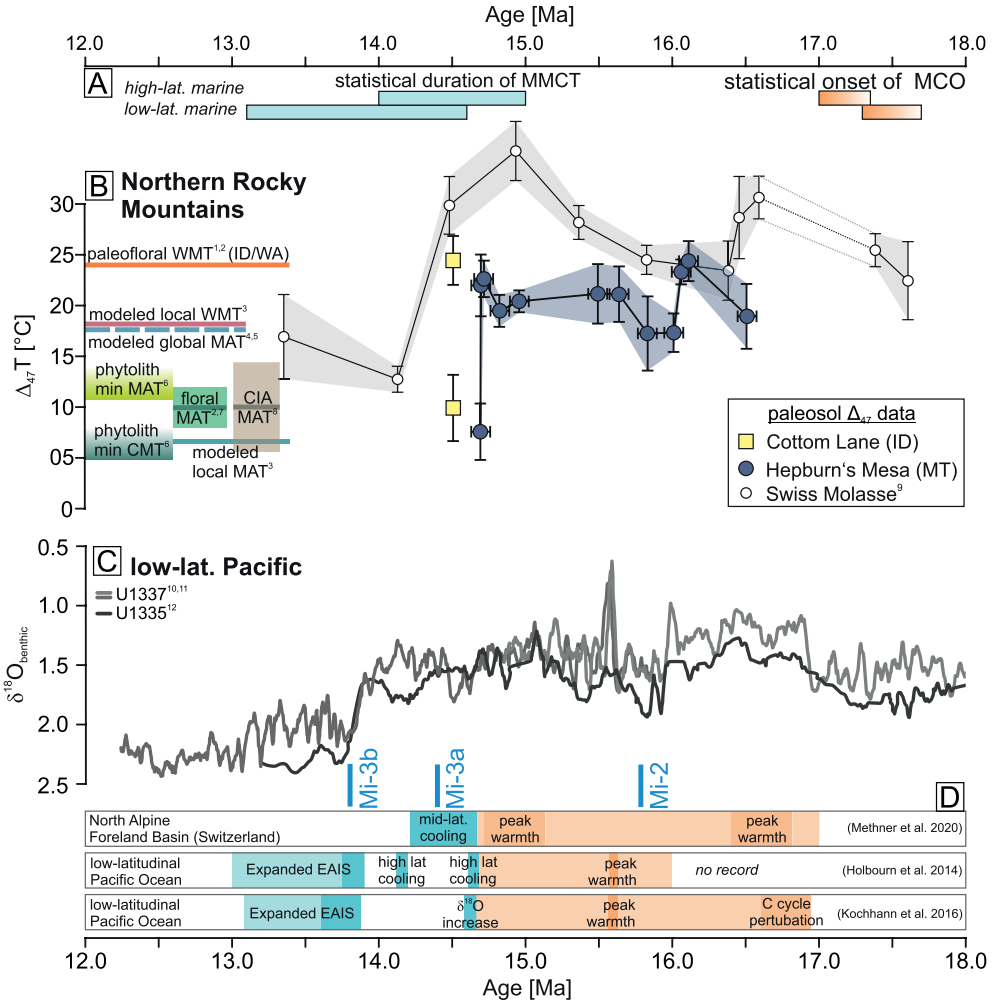

Figure 4. Comparison of terrestrial and marine MCO-MMCT records. (a) Statistical onset of the MCO and the duration of the MMCT (Mudelsee et al., 2014). (b) MCO Δ_{47}-temperature records of the Northern Rocky Mountains (Hepburn's Mesa and Cottom Lane localities, this study) and of the North Alpine Foreland Basin (Swiss Molasse Basin, Central Europe; 9: Methner et al., 2020) compared to phytolith-based mean annual temperatures (MAT) and cold month mean temperatures (CMT) (6: Harris et al., 2020) and soil chemical index of alteration-based MAT (7: Retallack, 2007), both from the nearby Railroad canyon section (ID) and paleofloral-based warm month temperatures (WMT) and MATs (Latah flora, E′ WA; 1–3: Chase et al., 1998; Wolfe, 1995; Wolfe & Hopkins, 1967). Modeled global MATs are from (4, 5: Goldner et al., 2014; You et al., 2009) and local MAT and summer temperatures (JJA) are extracted from (3: Zhou et al., 2018) for 3 × 3 grid cells around the sample locality. (c) Low-latitudinal Pacific $\delta^{18}O_{benthic}$ data (12–14: Holbourn et al., 2015; Kochhann et al., 2016; Tian et al., 2013), smoothed using the 9-point running average. Miocene isotope events after Miller and Mountain (1996). (d) Age ranges of temperature reconstructions of the Miocene Climatic Optimum (orange) and the Middle Miocene Climate Transition (blue) (Holbourn et al., 2014; Kochhann et al., 2016; Methner et al., 2020).

The NRM soil temperatures clearly exceed reconstructed early to middle Miocene MATs of 10°C–11°C from the nearby Railroad Canyon section (phytolith data, Harris et al., 2020; chemical index of alteration, Retallack, 2007) and 8°C–12°C from Northern Rocky Mountain floral assemblages (Chase et al., 1998; Wolfe, 1995) (Figure 3a). Paleosol carbonate Δ_{47}-temperatures may record a seasonal bias, most often suggested to reflect warm month temperatures (WMT) (Burgener et al., 2019; Gallagher et al., 2019; Hyland et al., 2018; Kelson et al., 2020; Methner et al., 2020; Passey et al., 2010; Peters et al., 2013; Quade et al., 2013). The soil matrix, the presence (or absence) and type of vegetation, as well as the timing of precipitation appear to be the main controls in modern and late Holocene soil carbonate Δ_{47}-temperatures that deviate from mean annual air temperatures (e.g., Gallagher & Sheldon, 2016; Kelson et al., 2020). Given the medium-to fine-grained sediments from which we recovered the analyzed paleosol carbonates (Figure 1) as

well as the ample evidence for vegetation in the NRM region (e.g., root cast in sections; phytolith analyses by Harris et al., 2020), and the regional semi-arid conditions (Harris et al., 2020; Retallack, 2007), the recovered Δ_{47}-temperatures should provide temperature estimates that rather reflect MATs (Gallagher & Sheldon, 2016; Kelson et al., 2020). However, based on comparison with local MAT estimates (Chase et al., 1998; Harris et al., 2020; Retallack, 2007; Wolfe, 1995) that are clearly colder than the deduced Δ_{47}-temperatures, we suggest that the latter rather reflect WMT. Independent (e.g., floral-based) WMT estimates are currently sparse for the NRM region. Only the Latah fossil leaf assemblage from eastern Washington provides a WMT estimate of ~24°C (MAT ~11°C, CMT ~0°C; Wolfe, 1995; Wolfe & Hopkins, 1967), but has been challenged to represent a low-elevation floral assemblage (Axelrod & Bailey, 1969). Modeled ground temperatures (Zhou et al., 2018), extracted for the paleogeographic position of the Hepburn's Mesa/NRM region (see supplementary information Section S3), show annual temperatures of 9°C and summer (JJA) temperatures of 21°C. This is in good agreement with local MAT proxy data (Chase et al., 1998; Harris et al., 2020; Retallack, 2007; Wolfe, 1995) and the mean soil temperatures of 21°C ± 2°C, thus reinforcing that the recovered paleosol carbonate temperature estimates likely reflect summer/WMT.

5.2. Environmental Conditions and Paleohydrology

Average paleosol $\delta^{13}C_c$ values of the NRM sections are −5.0 ± 0.8‰ (Hepburn's Mesa) and −5.9 ± 0.6‰ (Lemhi Valley). In the traditional carbon isotope framework such $\delta^{13}C_c$ values likely reflect mixed C3/C4 vegetation (Cerling, 1984; Cerling & Quade, 1993; Edwards et al., 2010). However, there is evidence for only minor amounts of C4 grasses in the NRM region (Railroad Canyon section; Harris, Strömberg, Sheldon, Smith, & Ibañez-Mejia, 2017), despite the increasing spread of open, grass-dominated habitats at the expense of forest cover during the early Miocene in the NRM region and the Great Plains (Harris, Strömberg, Sheldon, Smith, & Ibañez-Mejia, 2017; Strömberg, 2011). As such, the overall (semi-)arid conditions in the NRM region during the middle Miocene (Barnosky & Labar, 1989; Harris, Strömberg, Sheldon, Smith, & Ibañez-Mejia, 2017; Harris et al., 2020; Retallack, 2007; Strömberg, 2005; Thompson et al., 1982) may have caused reduced soil respiration rates and low productivity soils that result in the observed elevated $\delta^{13}C_c$ values despite only a small component of C4 vegetation (Caves et al., 2014; Cerling, 1984).

Similar to Δ_{47}-temperatures, the reconstructed $\delta^{18}O_{sw}$ values at Hepburn's Mesa lack any obvious trend throughout the MCO (Figure 3b). Reconstructed mean $\delta^{18}O_{sw}$ values of the Barstovian sites are −13.5 ± 1.2‰ (Hepburn's Mesa) and −14.1 ± 0.8‰ (Cottom Lane), yielding a mean $\delta^{18}O_{sw}$ value of −13.5 ± 1.2‰, which clearly contrasts with the very low Late Arikareean $\delta^{18}O_{sw}$ value of −17.8 ± 0.3‰ (Mollie Gulch). These low $\delta^{18}O_{sw}$ values at Mollie Gulch may be attributed to the lithology of the samples, likely reflecting shallow groundwater/deep soil horizons with dispersed carbonate (cf. Section 2.2, Figure 1e). Such carbonates are typically found in Renova Formation sediments and potentially reflect ground/soil waters derived from a larger catchment that includes rainfall from adjacent ranges and thus typically shows low $\delta^{18}O_{sw}$ values (Kent-Corson et al., 2006; Schwartz et al., 2019).

Interestingly, the Arikareean $\delta^{18}O_{sw}$ estimate (−17.8 ± 0.3‰; Mollie Gulch) is in agreement with reconstructed meteoric water $\delta^{18}O$ values based on tooth enamel samples from the same locality (median of ca −17‰; 1st time bin after Harris et al., 2020) (Figure 3b). Similarly, the youngest tooth enamel-based $\delta^{18}O$ estimate of ca. −14‰ (ca. 17–16 Ma, 5th time bin after Harris et al., 2020) agrees with our Barstovian $\delta^{18}O_{sw}$ estimate of −13.5 ± 1.2‰ (Cottom Lane and Hepburn's Mesa; Figure 3b).

Thus, as both proxies indicate a ~3‰–4‰ increase of reconstructed $\delta^{18}O$ values of meteoric/soil water in the NRM region, the shift between Arikareean (22.7–21.5 Ma) and Barstovian (16.9–14.7 Ma) carbonates may not simply be linked to lithological differences (groundwater vs. paleosol carbonate), but rather calls for a climatic and/or tectonic signal. We can currently only speculate about the reasons for this isotopic shift, but since local temperatures (this study; Harris et al., 2020; Retallack, 2007), precipitation amounts (Harris et al., 2020) and vegetation (Harris, Strömberg, Sheldon, Smith, & Ibañez-Mejia, 2017) remain relatively stable leading into the MCO, a ~3‰–4‰ increase of reconstructed $\delta^{18}O$ values may result from large-scale changes upstream and along the moisture trajectories or at the moisture source(s). On the other hand, changes in phytolith assemblages and diatom abundances indicate decreased water availability towards the MCO (Harris, Strömberg, Sheldon, Smith, & Ibañez-Mejia, 2017), and we cannot preclude local

drying/aridification in the NRM region during the Miocene Climatic Optimum even under stable temperature conditions.

5.3. MCO Temperature Conditions due to Continentality and Suppressed Westerlies

A strong marine—terrestrial (temperature) coupling during the middle Miocene is observed in near coastal settings in Europe (Donders et al., 2009; Methner et al., 2020), the Pacific North/Alaska (White et al., 1997), the U.S. Pacific coast (Wolfe, 1994), and even in Antarctica (Feakins et al., 2012). The only available paleosol Δ_{47}-temperature record of the MCO is from the Swiss Molasse Basin (Switzerland) and shows a synchronous pattern with marine paleoclimate records from the North Atlantic (Diester-Haass et al., 2009; Super et al., 2018), arguing for a strong coupling of the North Atlantic and Central European climate since the middle Miocene (Methner et al., 2020).

Both, the Swiss and the NRM Δ_{47}-temperatures exceed other proxy-derived MAT estimates by ca. 10°C and likely reflect northern hemisphere summer-biased/WMT Δ_{47}-temperatures. However, whereas this observation could be independently assessed by ample paleofloral-based WMT constraints for Central Europe (including the Swiss Molasse Basin), such data is largely lacking for the NRM region. Compared to the Swiss Δ_{47}-temperature record the NRM Δ_{47}-temperatures are colder (ca. 21°C compared to >24°C; Figure 4b), which is consistent with their high-elevation setting. Further, the NRM Δ_{47}-temperature does not recover the pronounced warm peaks at the beginning (ca. 16.5 Ma) and the end (ca. 14.9 Ma) of the MCO detected in the Swiss record (Figure 4b). More importantly unlike to the Swiss Δ_{47}-temperature record and paleofloral-based temperature records (White et al., 1997; Wolfe, 1994), we do not observe correlations to Pacific climate records (Figure 4).

We suggest that the generally colder and less variable NRM Δ_{47}-temperatures (spread of 7°C [17°C–24°C], average 21°C ± 2°C) are due to the different paleogeographic position of the intermontane basins of the NRM region, compared to the Swiss Molasse Basin (spread of 13°C [25°C–38°C], average 31°C ± 4°C; excluding MMCT samples [<14.8 Ma]). The Swiss Molasse Basin, as part of the large North Alpine Foreland Basin, reflects a low-elevation, likely densely vegetated (Böhme et al., 2007; Bruch et al., 2007), foreland basin with ample soil development on floodplain and overbank deposits of large alluvial mega-fan systems (Kälin & Kempf, 2009; Schlunegger et al., 2007). These fan systems developed in the vicinity to the retreating Molasse Sea north of the Alpine chain (Kuhlemann & Kempf, 2002) and most likely under direct influence of westerly North Atlantic air masses during the Miocene (Methner et al., 2020; Quan et al., 2014). In contrast, intermontane basins in the Northern Rocky Mountains developed at higher elevation (e.g., Chamberlain et al., 2012; Chase et al., 1998; Mix et al., 2011) delimited by mountain ranges (Barnosky & Labar, 1989; Constenius, 1996; Sears & Ryan, 2003), with small alluvial fans, braided river and saline lake deposits in an overall arid climate in open landscapes (Barnosky & Labar, 1989; Fields et al., 1985; Harris, Strömberg, Sheldon, Smith, & Ibañez-Mejia, 2017).

Overall, it appears that the global Miocene Climate signals, recorded in the marine sediments and Central European paleosols, are subdued in the high-elevation, continental NRM sites. This finding suggests that the prevailing westerlies were subordinate in controlling the recorded temperatures (via rainfall patterns) at the expense of local overall semi-arid and stable, mountain climate that apparently dominated the NRM region during the MCO. This result is in good agreement with stable environmental conditions leading into and during the beginning of the MCO reported from the Railroad Canyon section (Harris et al., 2020), but also throughout the MCO in the Mojave region (CA) (Loughney et al., 2019; Smiley et al., 2018). Middle Miocene paleoclimate models show an enhanced zonal flow at Northern Hemisphere mid-latitudes, supporting strong westerlies in western North America as well as in Europe (Herold et al., 2011; Krapp & Jungclaus, 2011). A modern rainfall-isotope study across the Canadian Cordillera shows that in times of enhanced zonal flow, both the rain shadow and the isotopic depletion of rainfall in the lee of the Canadian Cordillera is enhanced (Birks & Edwards, 2009). Assuming a similar behavior during the Miocene, a strong rain shadow could have suppressed westerlies. Collectively, a consistent picture emerges of relatively stable environmental conditions in continental western North America during the Miocene Climatic Optimum.

5.4. Temperature Variability at the End of the MCO

In the youngest part of the NRM Δ_{47}-temperature record (<15 Ma), we observe large "intra-horizon" Δ_{47}-temperature variability of ca. 14°C (Figures 3 and 4) at both sites, Hepburn's Mesa and Cottom Lane. Similarly large Δ_{47}-temperature swings, likely related to the onset of the MCCT occur in the European records, although these European records have much better age control (Swiss Molasse, Methner et al., 2020, Figure 4c; Central Spain, Löffler et al., 2019). Whereas the age constraints for the Cottom Lane locality are poor, the paleomagnetic section of Hepburn's Mesa currently places this temperature fluctuation at 14.7 Ma (see detailed age assignments in the supplementary information Section S1.2; Table 1). These temperature swings coincide with first high-latitudinal cooling steps after the MCO at ca. 14.7 Ma recorded in marine sediments of the Equatorial Pacific (Figure 4d) and the major shift in orbital pacing from eccentricity-dominated to obliquity-dominated cycles (Holbourn et al., 2013, 2014; Kochhann et al., 2016). We note that large and brief swings in paleosol Δ_{47}-temperatures occur at the onset of the MMCT (~14.8 Ma) at three different sites and settings, namely the low-elevation North Alpine Foreland Basin (Switzerland; Methner et al., 2020), the Calatayud-Daroca Basin (Spain; Löffler et al., 2019) and in the NRM region (this study). For the NRM region we are unable to provide the necessary temporal resolution to evaluate the rate and exact timing of these large temperature swings. The almost "intra-horizon" Δ_{47}-temperature variability suggests that temperature changes occurred over the duration of the actual carbonate accumulation time (~10^3–10^4 yr) in the NRM section, questioning orbital-forcing as a potential driver of these changes. Further, we cannot exclude that this "intra-horizon" variability is a more common feature throughout the section (and maybe even in other paleosol sections) that is typically missed due to the focus on temporal coverage at the expanse of spatial coverage. It demands a more detailed assessment of differences between samples from the apparently same soil horizon, for example, through dual clumped isotope analyses (e.g., Bajnai et al., 2020). Further sampling of MMCT sections at NRM localities will permit speculations if the transition from the global warmth of the MCO into the subsequent cooling of the MMCT is characterized by similarly large and brief terrestrial temperature swings as observed in the European records, possibly similar to the stepwise transition recorded in the global oceans (Diester-Haass et al., 2009; Holbourn et al., 2013, 2014; Super et al., 2018).

6. Conclusions

Our composite Northern Rocky Mountain paleosol record provides the first Δ_{47}-based temperature record of the Miocene Climatic Optimum in western North America. Temperature estimates are 21 ± 2°C, showing stable climate condition over much of the MCO until ca. 14.7 Ma, when "intra-horizon" Δ_{47}-temperatures become discrepant and we observe the first occurrence of rather low Δ_{47}-temperatures of 8°C–10°C that may be indicative of the onset of the MMCT. During the MCO Δ_{47}-temperatures exceed local mean annual temperatures proxy and model data (Harris et al., 2020; Herold et al., 2011; Retallack, 2007; Wolfe, 1995; Zhou et al., 2018) and likely represent dominantly WMT. Overall, we find that the NRM Δ_{47}-temperature record is largely dominated by inland continentality and stable temperature conditions throughout the Miocene Climatic Optimum.

Despite that spatial- and temporal-binned terrestrial temperature estimates indicate a pronounced MCO warming in western North America (Axelrod & Bailey, 1969; Mix & Chamberlain, 2014; Pound et al., 2012; White et al., 1997; Wolfe, 1994), more detailed paleoenvironmental and paleoclimate MCO records from USA inland sites (Mojave Desert and Northern Rocky Mountains) show overall stable climate and environmental condition (this study; Gallagher & Sheldon, 2013; Harris et al., 2020; Loughney et al., 2019; Retallack, 2007; Smiley et al., 2018). We, therefore, suggest that the (paleo)geographically distinct settings of the inland records, namely at high(er) elevation and/or in the lee of prominent mountain ranges (Sierra Nevada, (proto)-Cascades, Idaho Batholith, and incepting Yellowstone Hotspot), are responsible for the suppressed global MCO climate signal, typically recorded in marine and near-coastal, low-elevation settings, in favor of regional continental climates.

Data Availability Statement

Supplementary data to this article are additionally deposited at Zenodo (10.5281/zenodo.4659589).

Acknowledgments
We acknowledge assistance in the field by I. Yashchenko and J. Caves Rugenstein and in laboratory by S. Hofmann, C. Schreiber, and L. Jork. A. Barnosky kindly provided valuable information on the field sites. CPC acknowledges support through NSF EAR-1322084. JF acknowledges support through DFG FI 948/7-1. A. Mulch, K. Methner, and E. Krsnik acknowledge support through DFG-SPP 2017 4D-MB (MU 2845/6–1 and ME 4955/1–1). K. Methner further acknowledges support through the Alexander von Humboldt Foundation. We thank the Associate Editor, reviewer Ian Winkelstern, and an anonymous reviewer for their helpful comments that improved this manuscript. The authors declare no financial or any other conflict of interests. Open access funding enabled and organized by Projekt DEAL.

References

Axelrod, D. I., & Bailey, H. P. (1969). Paleotemperature analysis of tertiary floras. *Palaeogeography, Palaeoclimatology, Palaeoecology*, *6*, 163–195. https://doi.org/10.1016/0031-0182(69)90013-3

Bajnai, D., Guo, W., Spötl, C., Coplen, T. B., Methner, K., Löffler, N., et al. (2020). Dual clumped isotope thermometry resolves kinetic biases in carbonate formation temperatures. *Nature Communications*, *11*, 4005. https://doi.org/10.1038/s41467-020-17501-0

Barnosky, A. D., Bibi, F., Hopkins, S. S., & Nichols, R. (2007). Biostratigraphy and magnetostratigraphy of the mid-Miocene Railroad Canyon sequence, Montana and Idaho, and age of the mid-Tertiary unconformity west of the continental divide. *Journal of Vertebrate Paleontology*, *27*(1), 204–224. https://doi.org/10.1671/0272-4634(2007)27[204:bamotm]2.0.co;2

Barnosky, A. D., & Labar, W. J. (1989). Mid-Miocene (Barstovian) environmental and tectonic setting near Yellowstone Park, Wyoming and Montana. *The Geological Society of America Bulletin*, *101*(11), 1448–1456. https://doi.org/10.1130/0016-7606(1989)101<1448:mmbeat>2.3.co;2

Birks, S. J., & Edwards, T. W. D. (2009). Atmospheric circulation controls on precipitation isotope-climate relations in western Canada. *Tellus Series B: Chemical and Physical Meteorology*, *61*(3), 566–576. https://doi.org/10.1111/j.1600-0889.2009.00423.x

Blisniuk, P. M., & Stern, L. A. (2005). Stable isotope paleoaltimetry: A critical review. *American Journal of Science*, *305*(10), 1033–1074. https://doi.org/10.2475/ajs.305.10.1033

Böhme, M. (2003). The Miocene Climatic Optimum: Evidence from ectothermic vertebrates of Central Europe. *Palaeogeography, Palaeoclimatology, Palaeoecology*, *195*(3–4), 389–401. https://doi.org/10.1016/S0031-0182(03)00367-5

Böhme, M., Bruch, A. A., & Selmeier, A. (2007). The reconstruction of Early and Middle Miocene Climate and vegetation in Southern Germany as determined from the fossil wood flora. *Palaeogeography, Palaeoclimatology, Palaeoecology*, *253*(1–2), 91–114. https://doi.org/10.1016/j.palaeo.2007.03.035

Brand, W. A., Assonov, S. S., & Coplen, T. B. (2010). Correction for the ^{17}O interference in $\delta(^{13}C)$ measurements when analyzing CO_2 with stable isotope mass spectrometry (IUPAC Technical Report). *Pure and Applied Chemistry*, *82*(8), 1719–1733. https://doi.org/10.1351/PAC-REP-09-01-05

Breecker, D. O., & Retallack, G. J. (2014). Refining the pedogenic carbonate atmospheric CO_2 proxy and application to Miocene CO_2. *Palaeogeography, Palaeoclimatology, Palaeoecology*, *406*, 1–8. https://doi.org/10.1016/j.palaeo.2014.04.012

Bruch, A. A., Uhl, D., & Mosbrugger, V. (2007). Miocene Climate in Europe—Patterns and evolution: A first synthesis of NECLIME. *Palaeogeography, Palaeoclimatology, Palaeoecology*, *253*, 1–7. https://doi.org/10.1016/j.palaeo.2007.03.030

Burbank, A. D., & Barnosky, D. W. (1990). The magnetochronology of Barstovian mammals in southwestern Montana and implications for the initiation of Neogene crustal extension in the northern Rocky Mountains. *The Geological Society of America Bulletin*, *102*(8), 1093–1104. https://doi.org/10.1130/0016-7606(1990)102<1093:tmobmi>2.3.co;2

Burgener, L., Hyland, E., Huntington, K. W., Kelson, J. R., & Sewall, J. O. (2019). Revisiting the equable climate problem during the Late Cretaceous greenhouse using paleosol carbonate clumped isotope temperatures from the Campanian of the Western Interior Basin, USA. *Palaeogeography, Palaeoclimatology, Palaeoecology*, *516*, 244–267. https://doi.org/10.1016/j.palaeo.2018.12.004

Carrasco, M. A., Kraatz, B. P., Davis, E. B., & Barnosky, A. D. (2005). *Miocene mammal mapping project (MIOMAP)*. University of California Museum of Paleontology.

Caves, J. K., Sjostrom, D. J., Mix, H. T., Winnick, M. J., & Chamberlain, C. P. (2014). Aridification of Central Asia and uplift of the Altai and Hangay Mountains, Mongolia: Stable isotope evidence. *American Journal of Science*, *314*(8), 1171–1201. https://doi.org/10.2475/08.2014.01

Cerling, T. E. (1984). The stable isotopic composition of modern soil carbonate and its relationship to climate. *Earth and Planetary Science Letters*, *71*(2), 229–240. https://doi.org/10.1016/0012-821X(84)90089-X

Cerling, T. E., & Quade, J. (1993). Stable carbon and oxygen isotopes in soil carbonates. In P. K. Swart, K. C. Lohmann, J. Mckenzie, S. Savin, & Hrsg (Eds.), *Climate change in continental isotopic records (S. 217–231)*. American Geophysical Union.

Chamberlain, C. P., Mix, H. T., Mulch, A., Hren, M. T., Kent-Corson, M. L., Davis, S. J., et al. (2012). The Cenozoic climatic and topographic evolution of the western North American Cordillera. *American Journal of Science*, *312*(2), 213–262. https://doi.org/10.2475/02.2012.05

Chase, C. G., Gregory-Wodzicki, K. M., Totman Parrish, J., & DeCelles, P. G. (1998). *Topographic history of the western Cordillera of North American and controls on climate*. In T. J. Crowley, K. Burke, & Hrsg (Eds.), *Tectonic boundary conditions for climate reconstructions (S. 73–99)*. Oxford University Press.

Constenius, K. N. (1996). Late Paleogene extensional collapse of the Cordilleran foreland fold and thrust belt. *The Geological Society of America Bulletin*, *108*(1), 20–39. https://doi.org/10.1130/0016-7606(1996)108<0020:lpecot>2.3.co;2

Coplen, T. B. (2007). Calibration of the calcite–water oxygen-isotope geothermometer at Devils Hole, Nevada, a natural laboratory. *Geochimica et Cosmochimica Acta*, *71*(16), 3948–3957. https://doi.org/10.1016/j.gca.2007.05.028

Daëron, M., Blamart, D., Peral, M., & Affek, H. P. (2016). Absolute isotopic abundance ratios and the accuracy of Δ47 measurements. *Chemical Geology*, *442*, 83–96. https://doi.org/10.1016/j.chemgeo.2016.08.014

Dennis, K. J., Affek, H. P., Passey, B. H., Schrag, D. P., & Eiler, J. M. (2011). Defining an absolute reference frame for 'clumped' isotope studies of CO_2. *Geochimica et Cosmochimica Acta*, *75*(22), 7117–7131. https://doi.org/10.1016/j.gca.2011.09.025

De Vleeschouwer, D., Vahlenkamp, M., Crucifix, M., & Pälike, H. (2017). Alternating Southern and Northern Hemisphere climate response to astronomical forcing during the past 35 m. *Geology*, *45*(4), 375–378. https://doi.org/10.1130/G38663.1

Diester-Haass, L., Billups, K., Gröcke, D. R., François, L., Lefebvre, V., & Emeis, K. C. (2009). Mid-Miocene paleoproductivity in the Atlantic Ocean and implications for the global carbon cycle. *Paleoceanography*, *24*(1). https://doi.org/10.1029/2008PA001605

Donders, T. H., Weijers, J. W. H., Munsterman, D. K., Kloosterboer-van Hoeve, M. L., Buckles, L. K., Pancost, R. D., et al. (2009). Strong climate coupling of terrestrial and marine environments in the Miocene of northwest Europe. *Earth and Planetary Science Letters*, *281*(3–4), 215–225. https://doi.org/10.1016/j.epsl.2009.02.034

Edwards, E. J., Osborne, C. P., Strömberg, C. A., Smith, S. A., & C4 Grasses Consortium (2010). The origins of C4 grasslands: Integrating evolutionary and ecosystem science. *Science*, *328*(5978), 587–591. https://doi.org/10.1126/science.1177216

Fan, M., Ayyash, S. A., Tripati, A., Passey, B. H., & Griffith, E. M. (2017). Terrestrial cooling and changes in hydroclimate in the continental interior of the United States across the Eocene-Oligocene boundary. *Geological Society of America Bulletin*, *139*(7–8), 1073–1084. https://doi.org/10.1130/B31732.1

Feakins, S. J., Warny, S., & Lee, J.-E. (2012). Hydrologic cycling over Antarctica during the middle Miocene warming. *Nature Geoscience*, *5*(8), 557–560. https://doi.org/10.1038/ngeo1498

Fiebig, J., Bajnai, D., Löffler, N., Methner, K., Krsnik, E., Mulch, A., & Hofmann, S. (2019). Combined high-precision Δ_{48} and Δ_{47} analysis of carbonates. *Chemical Geology*, *522*, 186–191. https://doi.org/10.1016/j.chemgeo.2019.05.019

Fiebig, J., Hofmann, S., Löffler, N., Lüdecke, T., Methner, K., & Wacker, U. (2016). Slight pressure imbalances can affect accuracy and precision of dual inlet-based clumped isotope analysis. *Isotopes in Environmental and Health Studies*, *52*, 12–28. https://doi.org/10.1080/10256016.2015.1010531

Fields, R. W., Rasmussen, D. L., Tabrum, A. R., & Nichols, R. (1985). Cenozoic rocks of the intermontane basins of western Montana and eastern Idaho: A summary. In R. M. Flores, & S. S. Kaplan (Eds.), *Cenozoic paleogeography of the west-Central United States. Rocky mountain section (SEPM)*.

Flower, B. P., & Kennett, J. P. (1995). Middle Miocene deepwater paleoceanography in the southwest Pacific: Relations with East Antarctic Ice Sheet development. *Paleoceanography*, *10*(6), 1095–1112. https://doi.org/10.1029/95pa02022

Foster, G. L., Lear, C. H., & Rae, J. W. B. (2012). The evolution of pCO_2, ice volume and climate during the middle Miocene. *Earth and Planetary Science Letters*, *341–344*, 243–254. https://doi.org/10.1016/j.epsl.2012.06.007

Fritz, W. J., & Sears, J. W. (1993). Tectonics of the Yellowstone hotspot wake in, southwestern Montana. *Geology*, *21*(5), 427–430. https://doi.org/10.1130/0091-7613(1993)021<0427:totyhw>2.3.co;2

Fritz, W. J., Sears, J. W., McDowell, R. J., & Wampler, J. M. (2007). Cenozoic volcanic rocks of southwestern Montana. *Northwest Geology*, *36*, 91–110.

Gallagher, T. M., Hren, M., & Sheldon, N. D. (2019). The effect of soil temperature seasonality on climate reconstructions from Paleosols. *American Journal of Science*, *319*(7), 549–581. https://doi.org/10.2475/07.2019.02

Gallagher, T. M., & Sheldon, N. D. (2013). A new paleothermometer for forest paleosols and its implications for cenozoic climate. *Geology*, *41*(6), 647–650. https://doi.org/10.1130/G34074.1

Gallagher, T. M., & Sheldon, N. D. (2016). Combining soil water balance and clumped isotopes to understand the nature and timing of pedogenic carbonate formation. *Chemical Geology*, *435*, 79–91. https://doi.org/10.1016/j.chemgeo.2016.04.023

Goldner, A., Herold, N., & Huber, M. (2014). The challenge of simulating the warmth of the mid-Miocene Climatic Optimum in CESM1. *Climate of the Past*, *10*(2), 523–536. https://doi.org/10.5194/cp-10-523-2014

Hanneman, D. L., & Wideman, C. J. (2006). Calcic pedocomplexes—Regional sequence boundary indicators in Tertiary deposits of the Great Plains and western United States. *Geological Society of America Special Paper*, *416*, 1–15. https://doi.org/10.1130/2006.2416(01

Harris, E. B., Kohn, M. J., & Strömberg, C. A. E. (2020). Stable isotope compositions of herbivore teeth indicate climatic stability leading into the middle Miocene Climatic Optimum, in Idaho, U.S.A. *Palaeogeography, Palaeoclimatology, Palaeoecology*, 109610. https://doi.org/10.1016/j.palaeo.2020.109610

Harris, E. B., Strömberg, C. A. E., Sheldon, N. D., Smith, S. Y., & Vilhena, D. A. (2017). Vegetation response during the lead-up to the middle Miocene warming event in the Northern Rocky Mountains, USA. *Palaeogeography, Palaeoclimatology, Palaeoecology*, *485*, 401–415. https://doi.org/10.1016/j.palaeo.2017.06.029

Harris, E. B., Strömberg, C. A., Sheldon, N. D., Smith, S. Y., & Ibañez-Mejia, M. (2017). Revised chronostratigraphy and biostratigraphy of the early-middle Miocene Railroad Canyon section of central-eastern Idaho, USA. *GSA Bulletin*, *129*(9–10), 1241–1251. https://doi.org/10.1130/b31655.1

Herold, N., Huber, M., & Müller, R. D. (2011). Modeling the Miocene Climatic Optimum. Part I: Land and atmosphere. *Journal of Climate*, *24*(24), 6353–6372. https://doi.org/10.1175/2011JCLI4035.1

Hilgen, F. J., Lourens, L. J., Dam, Van, J. A., Beu, A. G., Boyes, A. F., Cooper, R. A., et al. (2012). Chapter 29—The Neogene Period. In *The geologic time scale* (S. 923–978). Elsevier.

Holbourn, A., Kuhnt, W., Clemens, S., Prell, W., & Andersen, N. (2013). Middle to late Miocene stepwise climate cooling: Evidence from a high-resolution deep water isotope curve spanning 8 million years. *Paleoceanography*, *28*(4), 688–699. https://doi.org/10.1002/2013PA002538

Holbourn, A., Kuhnt, W., Kochhann, K. G. D., Andersen, N., & Meier, K. J. S. (2015). Global perturbation of the carbon cycle at the onset of the Miocene Climatic Optimum. *Geology*, *43*(2), 123–126. https://doi.org/10.1130/g36317.1

Holbourn, A., Kuhnt, W., Lyle, M., Schneider, L., Romero, O., & Andersen, N. (2014). Middle Miocene Climate cooling linked to intensification of eastern equatorial Pacific upwelling. *Geology*, *42*(1), 19–22. https://doi.org/10.1130/g34890.1

Huntington, K. W., Wernicke, B. P., & Eiler, J. M. (2010). Influence of climate change and uplift on Colorado Plateau paleotemperatures from carbonate clumped isotope thermometry. *Tectonics*, *29*(3), TC3005. https://doi.org/10.1029/2009TC002449

Hyland, E. G., Huntington, K. W., Sheldon, N. D., & Reichgelt, T. (2018). Temperature seasonality in the North American continental interior during the early Eocene climatic optimum. *Climate of the Past*, *14*(10), 1391–1404. https://doi.org/10.5194/cp-14-1391-2018

Ivanov, D., Utescher, T., Mosbrugger, V., Syabryaj, S., Djordjević-Milutinović, D., & Molchanoff, S. (2011). Miocene vegetation and climate dynamics in Eastern and Central Paratethys (Southeastern Europe). *Palaeogeography, Palaeoclimatology, Palaeoecology*, *304*(3–4), 262–275. https://doi.org/10.1016/j.palaeo.2010.07.006

Kälin, D., & Kempf, O. (2009). High-resolution stratigraphy from the continental record of the Middle Miocene Northern Alpine Foreland Basin of Switzerland. *Neues Jahrbuch für Geologie und Paläontologie: Abhandlungen*, *254*(1–2), 177–235. https://doi.org/10.1127/0077-7749/2009/0010

Kelson, J. R., Huntington, K. W., Breecker, D. O., Burgener, L. K., Gallagher, T. M., Hoke, G. D., & Petersen, S. V. (2020). A proxy for all seasons? A synthesis of clumped isotope data from Holocene soil carbonates. *Quaternary Science Reviews*, *234*, 106259. https://doi.org/10.1016/j.quascirev.2020.106259

Kelson, J. R., Watford, D., Bataille, C., Huntington, K. W., Hyland, E., & Bowen, G. J. (2018). Warm terrestrial subtropics during the Paleocene and Eocene: Carbonate clumped isotope (Δ_{47}) evidence from the Tornillo Basin, Texas (USA). *Paleoceanography and Paleoclimatology*, *33*(11), 1230–1249. https://doi.org/10.1029/2018PA003391

Kendall, C., & Coplen, T. B. (2001). Distribution of oxygen-18 and deuterium in river waters across the United States. *Hydrological Processes*, *15*(7), 1363–1393. https://doi.org/10.1002/hyp.217

Kent-Corson, M. L., Barnosky, A. D., Mulch, A., Carrasco, M. A., & Chamberlain, C. P. (2013). Possible regional tectonic controls on mammalian evolution in western North America. *Palaeogeography, Palaeoclimatology, Palaeoecology*, *387*(0), 17–26. https://doi.org/10.1016/j.palaeo.2013.07.014

Kent-Corson, M. L., Sherman, L. S., Mulch, A., & Chamberlain, C. P. (2006). Cenozoic topographic and climatic response to changing tectonic boundary conditions in Western North America. *Earth and Planetary Science Letters*, *252*(3–4), 453–466. https://doi.org/10.1016/j.epsl.2006.09.049

Kim, S.-T., Mucci, A., & Taylor, B. E. (2007). Phosphoric acid fractionation factors for calcite and aragonite between 25°C and 75°C: revisited. *Chemical Geology*, *246*(3–4), 135–146. https://doi.org/10.1016/j.chemgeo.2007.08.005

Kim, S.-T., & O'Neil, J. R. (1997). Equilibrium and nonequilibrium oxygen isotope effects in synthetic carbonates. *Geochimica et Cosmochimica Acta*, *61*(16), 3461–3475. https://doi.org/10.1016/S0016-7037(97)00169-5

Kochhann, K. G. D., Holbourn, A., Kuhnt, W., Channell, J. E. T., Lyle, M., Shackford, J. K., et al. (2016). Eccentricity pacing of eastern equatorial Pacific carbonate dissolution cycles during the Miocene Climatic Optimum. *Paleoceanography*, *31*(9), 1176–1192. https://doi.org/10.1002/2016PA002988

Krapp, M., & Jungclaus, J. H. (2011). The Middle Miocene Climate as modeled in an atmosphere-ocean-biosphere model. *Climate of the Past*, *7*(4), 1169–1188. https://doi.org/10.5194/cp-7-1169-2011

Kuhlemann, J., & Kempf, O. (2002). Post-Eocene evolution of the North Alpine Foreland Basin and its response to Alpine tectonics. *Sedimentary Geology*, *152*(1–2), 45–78. https://doi.org/10.1016/S0037-0738(01)00285-8

Kürschner, W. M., Kvaček, Z., & Dilcher, D. L. (2008). The impact of Miocene atmospheric carbon dioxide fluctuations on climate and the evolution of terrestrial ecosystems. *Proceedings of the National Academy of Sciences*, *105*(2), 449–453. https://doi.org/10.1073/pnas.0708588105

Larsson, L. M., Dybkjær, K., Rasmussen, E. S., Piasecki, S., Utescher, T., & Vajda, V. (2011). Miocene Climate evolution of northern Europe: A palynological investigation from Denmark. *Palaeogeography, Palaeoclimatology, Palaeoecology*, *309*(3–4), 161–175. https://doi.org/10.1016/j.palaeo.2011.05.003

Lear, C. H., Coxall, H. K., Foster, G. L., Lunt, D. J., Mawbey, E. M., Rosenthal, Y., et al. (2015). Neogene ice volume and ocean temperatures: Insights from infaunal foraminiferal Mg/Ca paleothermometry. *Paleoceanography*, *30*(11), 1437–1454. https://doi.org/10.1002/2015PA002833

Löffler, N., Fiebig, J., Krijgsman, W., & Mulch, A. (2019). *The magnitude of continental temperature change during the middle Miocene Climatic Transition in Southern Europe*. AGU Fall Meeting Abstracts PP14A-08.

Loughney, K. M., Hren, M. T., Smith, S. Y., & Pappas, J. L. (2019). Vegetation and habitat change in southern California through the middle Miocene Climatic Optimum: Paleoenvironmental records from the Barstow Formation, Mojave Desert, USA. *Geological Society of America Bulletin*

Methner, K., Campani, M., Fiebig, J., Löffler, N., Kempf, O., & Mulch, A. (2020). Middle Miocene long-term continental temperature change in and out of pace with marine climate records. *Scientific Reports*, *10*(1), 7989. https://doi.org/10.1038/s41598-020-64743-5

Methner, K., Mulch, A., Fiebig, J., Wacker, U., Gerdes, A., Graham, S. A., & Chamberlain, C. P. (2016). Rapid Middle Eocene temperature change in western North America. *Earth and Planetary Science Letters*, *450*, 132–139. https://doi.org/10.1016/j.epsl.2016.05.053

Miller, K. G., & Mountain, G. S. (1996). Drilling and dating New Jersey Oligocene-Miocene sequences: Ice volume, global sea level, and Exxon records. *Science*, *271*(5252), 1092–1095. https://doi.org/10.1126/science.271.5252.1092

Miller, K. G., Wright, J. D., & Fairbanks, R. G. (1991). Unlocking the ice house: Oligocene-Miocene oxygen isotopes, eustasy, and margin erosion. *Journal of Geophysical Research*, *96*(B4), 6829–6848. https://doi.org/10.1029/90jb02015

Mix, H. T., & Chamberlain, C. P. (2014). Stable isotope records of hydrologic change and paleotemperature from smectite in Cenozoic western North America. *Geochimica et Cosmochimica Acta*, *141*(0), 532–546. https://doi.org/10.1016/j.gca.2014.07.008

Mix, H. T., Mulch, A., Kent-Corson, M. L., & Chamberlain, C. P. (2011). Cenozoic migration of topography in the North American Cordillera. *Geology*, *39*(1), 87–90. https://doi.org/10.1130/g31450.1

Mudelsee, M., Bickert, T., Lear, C. H., & Lohmann, G. (2014). Cenozoic climate changes: A review based on time series analysis of marine benthic $\delta^{18}O$ records. *Reviews of Geophysics*, *52*(3), 333–374. https://doi.org/10.1002/2013RG000440

Passey, B. H., Levin, N. E., Cerling, T. E., Brown, F. H., & Eiler, J. M. (2010). High-temperature environments of human evolution in East Africa based on bond ordering in paleosol carbonates. *Proceedings of the National Academy of Sciences*, *107*(25), 11245–11249. https://doi.org/10.1073/pnas.1001824107

Petersen, S. V., Defliese, W. F., Saenger, C., Daëron, M., Huntington, K. W., John, C. M., et al. (2019). Effects of improved ^{17}O correction on interlaboratory agreement in clumped isotope calibrations, estimates of mineral-specific offsets, and temperature dependence of acid digestion fractionation. *Geochemistry, Geophysics, Geosystems*, *20*(7), 3495–3519. https://doi.org/10.1029/2018gc008127

Peters, N. A., Huntington, K. W., & Hoke, G. D. (2013). Hot or not? Impact of seasonally variable soil carbonate formation on paleotemperature and O-isotope records from clumped isotope thermometry. *Earth and Planetary Science Letters*, *361*(0), 208–218. https://doi.org/10.1016/j.epsl.2012.10.024

Pound, M. J., Haywood, A. M., Salzmann, U., & Riding, J. B. (2012). Global vegetation dynamics and latitudinal temperature gradients during the Mid to Late Miocene (15.97–5.33 Ma). *Earth-Science Reviews*, *112*(1), 1–22. https://doi.org/10.1016/j.earscirev.2012.02.005

Quade, J., Eiler, J., Daëron, M., & Achyuthan, H. (2013). The clumped isotope geothermometer in soil and paleosol carbonate. *Geochimica et Cosmochimica Acta*, *105*(0), 92–107. https://doi.org/10.1016/j.gca.2012.11.031

Quan, C., Liu, Y.-S., Tang, H., & Utescher, T. (2014). Miocene shift of European atmospheric circulation from trade wind to westerlies. *Scientific Reports*, *4*, 5660. https://doi.org/10.1038/srep05660

Retallack, G. J. (2007). Cenozoic paleoclimate on land in North America. *The Journal of Geology*, *115*(3), 271–294. https://doi.org/10.1086/512753

Schlunegger, F., Rieke-Zapp, D., & Ramseyer, K. (2007). Possible environmental effects on the evolution of the Alps-Molasse Basin system. *Swiss Journal of Geosciences*, *100*(3), 383–405. https://doi.org/10.1007/s00015-007-1238-9

Schwartz, T. M., Methner, K., Mulch, A., Chamberlain, C. P., & Graham, S. A. (2019). Paleogene topographic and climatic evolution of the Northern Rocky Mountains from integrated sedimentary and isotopic data. *GSA Bulletin*, *131*(7–8), 1203–1223. https://doi.org/10.1130/b32068.1

Sears, J. W., Hendrix, M. S., Thomas, R. C., & Fritz, W. J. (2009). Stratigraphic record of the Yellowstone hotspot track, Neogene Sixmile Creek Formation grabens, southwest Montana. *Journal of Volcanology and Geothermal Research*, *188*(1–3), 250–259. https://doi.org/10.1016/j.jvolgeores.2009.08.017

Sears, J. W., & Ryan, P. C. (2003). Cenozoic evolution of the Montana Cordillera: Evidence from Paleovalleys. In R. G. Raynolds, R. M. Flores (Hrsg) (Eds.), *Cenozoic systems of the Rocky mountain region (S. 289–301)*. The Rocky Mountain Section (SEPM).

Smiley, C. J., Gray, J., & Huggins, L. M. (1975). Preservation of Miocene fossils in unoxidized lake deposits, Clarkia, Idaho; with a section on fossil insecta by W. F. Barr and J. M. Gillespie. *Journal of Paleontology*, *49*(5), 833–844.

Smiley, T. M., Hyland, E. G., Cotton, J. M., & Reynolds, R. E. (2018). Evidence of early C4 grasses, habitat heterogeneity, and faunal response during the Miocene Climatic Optimum in the Mojave Region. *Palaeogeography, Palaeoclimatology, Palaeoecology*, *490*, 415–430. https://doi.org/10.1016/j.palaeo.2017.11.020

Snell, K. E., Thrasher, B. L., Eiler, J. M., Koch, P. L., Sloan, L. C., & Tabor, N. J. (2013). Hot summers in the Bighorn Basin during the early Paleogene. *Geology*, *41*(1), 55–58. https://doi.org/10.1130/g33567.1

Sosdian, S. M., Babila, T. L., Greenop, R., Foster, G. L., & Lear, C. H. (2020). Ocean carbon storage across the middle Miocene: A new interpretation for the Monterey Event. *Nature Communications*, *11*(1), 134. https://doi.org/10.1038/s41467-019-13792-0

Sosdian, S. M., Greenop, R., Hain, M. P., Foster, G. L., Pearson, P. N., & Lear, C. H. (2018). Constraining the evolution of Neogene ocean carbonate chemistry using the boron isotope pH proxy. *Earth and Planetary Science Letters*, *498*, 362–376. https://doi.org/10.1016/j.epsl.2018.06.017

Steinthorsdottir, M., Jardine, P. E., & Rember, W. C. (2021). Near-future pCO_2 during the hot Miocene Climatic Optimum. *Paleoceanography and Paleoclimatology*, *36*(1). https://doi.org/10.1029/2020PA003900

Strömberg, C. A. E. (2005). Decoupled taxonomic radiation and ecological expansion of open-habitat grasses in the Cenozoic of North America. *Proceedings of the National Academy of Sciences of the United States of America*, *102*(34), 11980–11984. https://doi.org/10.1073/pnas.0505700102

Strömberg, C. A. E. (2011). Evolution of grasses and grassland ecosystems. *Annual Review of Earth and Planetary Sciences*, *39*(1), 517–544. https://doi.org/10.1146/annurev-earth-040809-152402

Super, J. R., Thomas, E., Pagani, M., Huber, M., O'Brien, C. L., & Hull, P. M. (2020). Miocene evolution of North Atlantic sea surface temperature. *Paleoceanography and Paleoclimatology*, *35*(5). https://doi.org/10.1029/2019PA003748

Super, J. R., Thomas, E., Pagani, M., Huber, M., O'Brien, C., & Pincelli, M. H. (2018). North Atlantic temperature and pCO_2 coupling in the early-middle Miocene. *Geology*, *46*(6), 519–522. https://doi.org/10.1130/G40228.1

Tedford, R. H., Albright, L. B., Barnosky, A. D., Ferrusquia-Villafranca, I., Hunt, R. M., Storer, J. E., et al. (2004). *Mammalian biochronology of the Arikareean through Hemphillian interval (late Oligocene through early Pliocene epochs)*. In *Late cretaceous and cenozoic mammals of North America: Biostratigraphy and geochronology* (pp. 169–231). New York: Columbia University Press. https://doi.org/10.7312/wood13040-008

Thompson, G. R., Fields, R. W., & Alt, D. (1982). Land-based evidence for Tertiary climatic variations: Northern Rockies. *Geology*, *10*(8), 413–417. https://doi.org/10.1130/0091-7613(1982)10<413:leftcv>2.0.co;2

Tian, J., Yang, M., Lyle, M. W., Wilkens, R., & Shackford, J. K. (2013). Obliquity and long eccentricity pacing of the Middle Miocene climate transition. *Geochemistry, Geophysics, Geosystems*, *14*(6), 1740–1755. https://doi.org/10.1002/ggge.20108

Wacker, U., Fiebig, J., Tödter, J., Schöne, B. R., Bahr, A., Friedrich, O., et al. (2014). Empirical calibration of the clumped isotope paleothermometer using calcites of various origins. *Geochimica et Cosmochimica Acta*, *141*(0), 127–144. https://doi.org/10.1016/j.gca.2014.06.004

Wang, H., Leng, Q., Liu, W., & Yang, H. (2017). A rapid lake-shallowing event terminated preservation of the Miocene Clarkia Fossil Konservat-Lagerstätte (Idaho, USA). *Geology*, *45*(3), 239–242. https://doi.org/10.1130/G38434.1

White, J. M., Ager, T. A., Adam, D. P., Leopold, E. B., Liu, G., Jetté, H., & Schweger, C. E. (1997). An 18 million year record of vegetation and climate change in northwestern Canada and Alaska: Tectonic and global climatic correlates. *Palaeogeography, Palaeoclimatology, Palaeoecology*, *130*(1–4), 293–306. https://doi.org/10.1016/S0031-0182(96)00146-0

Wolfe, J. A. (1994). Tertiary climatic changes at middle latitudes of western North America. *Palaeogeography, Palaeoclimatology, Palaeoecology*, *108*(3–4), 195–205. https://doi.org/10.1016/0031-0182(94)90233-X

Wolfe, J. A. (1995). Paleoclimatic estimates from Tertiary leaf assemblages. *Annual Review of Earth and Planetary Sciences*, *23*, 119–142. https://doi.org/10.1146/annurev.ea.23.050195.001003

Wolfe, J. A., & Hopkins, D. M. (1967). Climatic changes recorded by Tertiary land floras in northwestern North America. In *Tertiary Correlations and Climatic Changes in the Pacific 11th Pacific Science Symposium* (Vol. 25, pp. 67–76).

You, Y., Huber, M., Müller, R. D., Poulsen, C. J., & Ribbe, J. (2009). Simulation of the middle Miocene Climate Optimum. *Geophysical Research Letters*, *36*(4). https://doi.org/10.1029/2008GL036571

Zachos, J. C., Dickens, G. R., & Zeebe, R. E. (2008). An early Cenozoic perspective on greenhouse warming and carbon-cycle dynamics. *Nature*, *451*(7176), 279–283. https://doi.org/10.1038/nature06588

Zachos, J. C., Pagani, M., Sloan, L., Thomas, E., & Billups, K. (2001). Trends, rhythms, and aberrations in global climate 65 Ma to present. *Science*, *292*(5517), 686–693. https://doi.org/10.1126/science.1059412

Zhang, Y. G., Pagani, M., Liu, Z., Bohaty, S. M., & DeConto, R. (2013). A 40-million-year history of atmospheric CO_2. *Philosophical Transactions of the Royal Society A: Mathematical, Physical & Engineering Sciences*, *371*(2001). https://doi.org/10.1098/rsta.2013.0096

Zhou, H., Helliker, B. R., Huber, M., Dicks, A., & Akçay, E. (2018). C4 photosynthesis and climate through the lens of optimality. *Proceedings of the National Academy of Sciences*, *115*(47), 12057–12062. https://doi.org/10.1073/pnas.1718988115

References From the Supporting Information

Ingalls, M., & Snell, K. E. (2021). Tools for comprehensive assessment of fluid-mediated and solid-state alteration of carbonates used to reconstruct ancient elevation and environments. *Frontiers of Earth Science*, *9*, 623982. https://doi.org/10.3389/feart.2021.623982

Merritt, D. A., & Hayes, J. M. (1994). Factors controlling precision and accuracy in isotope-ratio-monitoring mass spectrometry. *Analytical Chemistry*, *66*, 2336–2347. https://doi.org/10.1021/ac00086a020

Passey, B. H., & Henkes, G. A. (2012). Carbonate clumped isotope bond reordering and geospeedometry. *Earth and Planetary Science Letters*, *351–352*, 223–236. https://doi.org/10.1016/j.epsl.2012.07.021

Vickers, M. L., Bajnai, D., Price, G. D., Linckens, J., & Fiebig, J. (2019). Southern high-latitude warmth during the Jurassic–Cretaceous: New evidence from clumped isotope thermometry. *Geology*, *47*, 724–728. https://doi.org/10.1130/G46263.1